Development of a cooling and power generation prototype integrating an axial micro-turbine in an absorption chiller

Simone Braccio, Nolwenn Le Pierrès, Nicolas Tauveron, Bertrand Chandez, Hai Trieu Phan

Version of Record: https://www.sciencedirect.com/science/article/pii/S1359431123010554
Manuscript_a341dae7ccd70073bf1157cb729b5e76

Development of a cooling and power generation prototype integrating an axial micro-turbine in an absorption chiller

Simone Braccio[1, 2], Nolwenn Le Pierrès[2], Nicolas Tauveron[1], Bertrand Chandez[1], Hai Trieu Phan[1,*]

[1] *Univ. Grenoble Alpes, CEA, Liten, Campus Ines, 73375 Le Bourget du Lac, France*

[2]*LOCIE, Univ. Savoie Mont Blanc, CNRS UMR5271, Savoie Technolac, 73376 Le Bourget Du Lac, France*

**Corresponding author: Haitrieu.PHAN@cea.fr*

ARTICLE INFO

Keywords:
Combined absorption power-cooling cycle
Experimental prototype
Ammonia-water
Low grade heat

HIGHLIGHTS

- Development of a combined absorption cooling and electricity production pilot plant
- Integration of a partial admission axial impulse micro-turbine in an absorption chiller
- Linear dependency of turbine mass flow rate from inlet pressure
- Strong interconnections between the cooling and power production lines
- Turbine line opening significantly increases circulating vapour mass flow rate

ABSTRACT

The integration of an expander in an absorption machine allows it to produce cooling and electricity simultaneously within the same cycle. This technology holds great potential to harness low-temperature heat sources more efficiently than production with separate cycles. However, very few experimental studies on absorption combined cooling and power production cycles can be found in literature. In order to achieve an in-depth understanding of this technology and of the interactions between power and cooling production sides of the circuit, the integration of an expander into a single stage ammonia water absorption chiller was undertaken through the development of an experimental pilot plant. The peculiar characteristics of the expansion device, as well as the use of a newly developed combined desorber avoiding the presence of a rectifier make the prototype built unique. Design and integration of the expander proved to be very challenging, mainly due to the small size of the application and corrosiveness of the ammonia water mixture. Significant electricity generation losses experienced lead to maximum electrical efficiency of 7% and corresponding maximum power production around 33 W at a lower than expected rotational speed of 20'000 rpm.

Despite these difficulties, first experimental measurements have been obtained, giving interesting insights on the functioning of the cycle. Indeed, the impracticability of regulating the ratio between cooling and power production was highlighted, due to the characteristics of the impulse turbine. Opening of the turbine line in the nominal point leads to a reduction of the mass flow rate passing through the cooling line of 65% (i.e., split ratio of 0.35) and a cooling power output decrease of around 57% (from 4.9 to 2.1 kW). Additionally, diverting some of the desorbed vapour to the power production line has important effects on the pressure equilibrium and circulating vapour mass flow rate, increasing from 16.1 kg/h in the simple absorption working mode to 31.1 kg/h in the combined mode in the nominal operating point. Feedback from the pilot plant will be very useful for the further development of the technology.

Nomenclature

A	section	[m²]	D_S	specific diameter	
D	diameter	[m]	*HTF*	heat transfer fluid	
h	specific enthalpy	[J.kg^{-1}]	*ORC*	organic Rankine cycle	
$\dot{m}$	mass flow rate	[kg. s^{-1}]	N_S	specific speed	
P	pressure	[bar]	r_S	split ratio	
Q	vapour quality	[-]			
$\dot{Q}$	thermal power	[kW]	*Subscripts and superscripts*		
r_s	Split ratio	[-]	*a*	absorber	
R	ideal gas constant	[J. K^{-1} mol^{-1}]	*c*	condenser	
R1,R2,R3	electrical resistances	[Ω]	d	desorber	
s	specific entropy	[J. K^{-1}. kg^{-1}]	*e*	evaporator, electric	
T	temperature	[°C]	*el*	electric	
$\dot{W}$	mechanical power	[W]	*fluid*	fluid	
x	ammonia mass fraction	[-]	*in*	inlet	
			is	isentropic	
Greek letters			*max*	maximum	
γ	gas adiabatic index	[-]	*out*	outlet	
Δ	variation	[-]	*rect*	rectifier	
η	efficiency	[-]	*shx*	solution heat exchanger	
ρ	density	[kg.m^{-3}]	*sub*	subcooler	
ω	rotational speed	[rpm]	*sh*	superheater	
			t	turbine	
Acronyms			*throat*	throat	
ACP	absorption cooling and power		*tot*	total	
COP	coefficient of performance		*1,2,..,17*	state points	

1. Introduction

In view of increasing global energy demand and concern for the environment, the scientific community continues to focus its efforts on the search for more efficient energy conversion technologies based on energy recovery and renewable resources. Of particular concern is the increasing demand for cooling, which is expected to triple globally from 2016 until 2050 [1] due to climate change and increasing population. In this context, absorption systems [2], which have been a relatively niche technology so far, are well suited to the recovery of low temperature energy for the production of cooling [3]. Research has focused on improving the performance of thermal cooling systems by combining power cycles, such as the Kalina cycle [4] or the Rankine cycle [5], with absorption cycles to produce both cooling and power using only one heat source rather than coupling two cycles in cascade. This can lead to an increased system efficiency and more effective usage of the heat source [6], as well as the mutualisation of components for vapour generation, condensation, pumping, etc. A combined absorption system producing not only refrigeration but also electricity could be better adapted to the whole range of energy demand, from only power to only cooling working modes, with intermediate operation modes producing different ratios of the two products.

While several analyses were performed on combined power and cooling cycles, most of them are generally limited to high heat source temperatures [7]–[9] or complex architectures [9]. Most of the studies available in literature involve simple modelling of the expander, usually assuming fixed isentropic efficiencies and the possibility to regulate the ratio between cooling and power production.
Additionally, a lack of experimental studies on absorption based combined cooling and electricity production cycles can be highlighted. Most of these studies were performed on series architectures and in particular on the Goswami cycle [10]. Tamm et al. [11] constructed a prototype (details about the size are not available) to demonstrate the feasibility of the Goswami cycle and to compare experimental results with numerical simulations. Deviations from ideal modelling were highlighted, but the potential for combined power and refrigeration output was demonstrated.
Han et al. [12] built an experimental rig for combined refrigeration and power production using a parallel architecture. The system, using the ammonia-water mixture could work in simple absorption refrigeration mode and absorption refrigeration and power production mode. The design cooling capacity in refrigeration mode was 10 kW and the design power capacity in power generation mode 2 kW. However, the authors claimed that no expander was available on the market for the small-scale experimental prototype. Hence, they simulated the expander using a throttling valve and a vapour heat exchanger. The same method of simulating the expander was also used in the aforementioned Goswami cycle prototype developed by Tamm et al. [11] and Kumar et al. [13].
The expander selection is of paramount importance for the efficiency of the system, but it is complicated by the small scales of experimental prototype (less than1 kWe) and by the use of the ammonia-water mixture, a very corrosive fluid. This requires the development of suitable expansion devices for absorption based combined cycles and complicates the development of experimental prototypes. Nevertheless, experimental studies are crucial in order to fully understand this technology and, in particular, the interactions between the expander and the cycle that integrates it. Considering the strong interconnections between the two production lines, it is important to investigate the functioning of the machine as the two products outputs vary, as well as during transient operation and performance in different operating modes.

To bring an advancement on the subject, the objective of the present study was the development of a suitable expander for a small-scale absorption combined cooling and power (ACP) cycle and its integration in a single stage ammonia water absorption chiller. The particular characteristics of the chosen expander (a supersonic partial admission axial micro-turbine) as well as the use of a newly developed component able to desorb and purify the ammonia vapour make the developed prototype unique.
The work is based on an existing absorption chiller pilot plant, with a desorber thermal power of 10 kW to which a turbine is integrated for operation in combined production mode. In a previous study [14], a scroll type volumetric expander was found to be unsuitable for such a small application, due to an excessive leakage rate. A different power generation technology is therefore investigated here, that of a partial admission impulse axial turbo-expander. The fact that in this type of expander all the expansion takes place in the injector limits the influence of leaking losses and guarantees a good level of work output [15]. However, due to the intrinsic behaviour of the turbine, special attention must be paid to the interdependencies between the physics governing the expander and the cycle that integrates it.

Design and integration of the expander proved to be very challenging, mainly due to the small size of the application and corrosiveness of the ammonia water mixture. Even though the technical challenges and the problems encountered in the setting up of the pilot plant did not allow its complete characterisation, combined cooling and power generation was achieved and the possibility to switch between different working modes was proved.

Hence, the main contribution of the present work is to bring thus far missing experimental data on a small scale axial turbine working with ammonia, as well as its integration into an absorption chiller prototype proving the possibility of generating variable ratios of cooling and electricity using this technology. The analyses carried out in this study give important insights on the functioning and limitations of this cycle, as well as on the challenges and difficulties of performing experimental investigation at such small scale. Experience and feedback from the prototype will play an important role for the future improvement of the technology.

2. Description of the cycle

The combined cooling and power cycle under investigation is shown schematically in **Fig. 1**. The functioning is based on an ammonia-water absorption machine with an expander coupled in parallel to the cooling production circuit. This type of architecture was chosen because of the greater flexibility it allows in choosing between cooling and electricity production [10].

On the solution loop, a first line of solution rich in ammonia circulates from the absorber to the desorber and is pressurised by a pump (points 1-2). A second line comprising an expansion valve returns the poor solution to the absorber (point 6). The solution heat exchanger preheats the rich solution (points 2-3) with the poor solution leaving the desorber (points 4-5) where a supply of heat at high temperature enables the desorption of vapour (point 7), mainly consisting of ammonia, from the solution. On the electricity production line, the expander selection process leads to the choice of an axial partial-admission impulse turbine (points 15-16) for production of the power $\dot{W}_T$. Before the turbine, a superheater (points 14-15) supplies the power $\dot{Q}_{sh}$ to increase the temperature of the fluid and ensure that it remains in the vapour state throughout the expansion which occurs inside the turbine. Indeed, condensation of the mixture during the expansion would be detrimental to the functioning of the expander and could lead to its rupture.

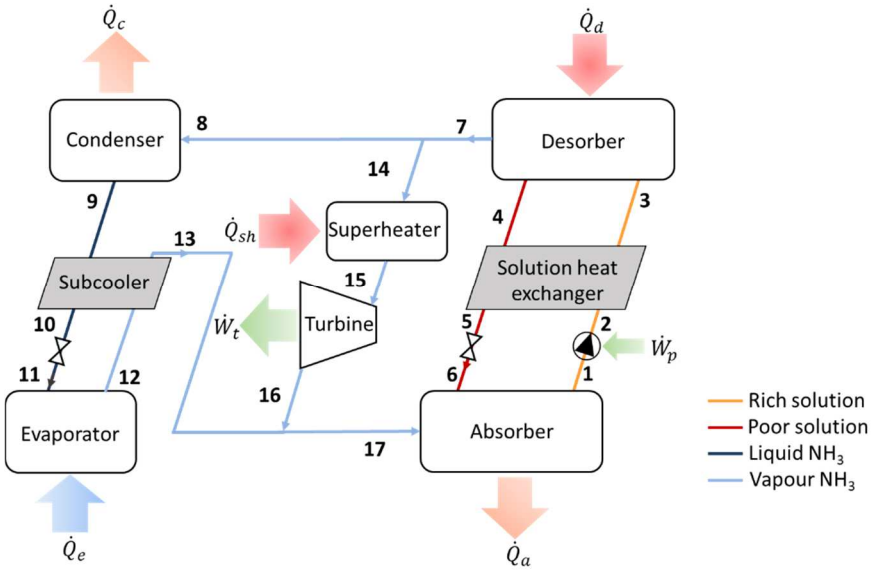

Fig. 1. Schematic diagram of the ACP cycle.

On the cooling production line, ammonia is condensed (points 8-9) through the exchange of the thermal power $\dot{Q}_c$ with an intermediate temperature source. Before cooling the cold source at the evaporator (points 11-12) by absorbing the power $\dot{Q}_e$, the fluid is expanded in a valve to achieve low pressure. A sub-cooler is used to pre-cool the ammonia (points 9-10) before it expands using the ammonia coming out of the evaporator. The ammonia flows of the two cooling and electricity production lines mix (point 17) and are ultimately absorbed in the poor solution due to cooling by an intermediate temperature source (the same as used for the condenser) to which the power $\dot{Q}_a$ is transferred.

3. Experimental prototype

3.1. Absorption chiller prototype

The prototype (shown in **Fig. 2**) development is based on an existing thermally driven single-effect ammonia-water absorption chiller of 7 kW cooling capacity.

Since the ammonia-water mixture is corrosive to most common materials, only stainless steel and EPDM or PTFE for seals and membranes are used in the prototype. In order to increase the compactness and reduce the cost of the prototype, commercial brazed/welded plate heat exchangers are used. Particular attention was paid also to the selection of the pump, the major electricity consuming component of the cycle. Since the liquid solution entering the pump comes from the absorber, its temperature is relatively close to saturation and desorption around the moving parts might occur in the presence of frictional heating. As this could severely reduce its lifespan, the pump must show very little heating, even locally. These considerations lead to the selection of a *Hydra-Cell*® diaphragm triplex single-acting pump, driven by an induction motor coupled to a variable frequency drive for flow control. Performance evaluation of the pump integrated in the cycle was performed by Landelle et al. [16].

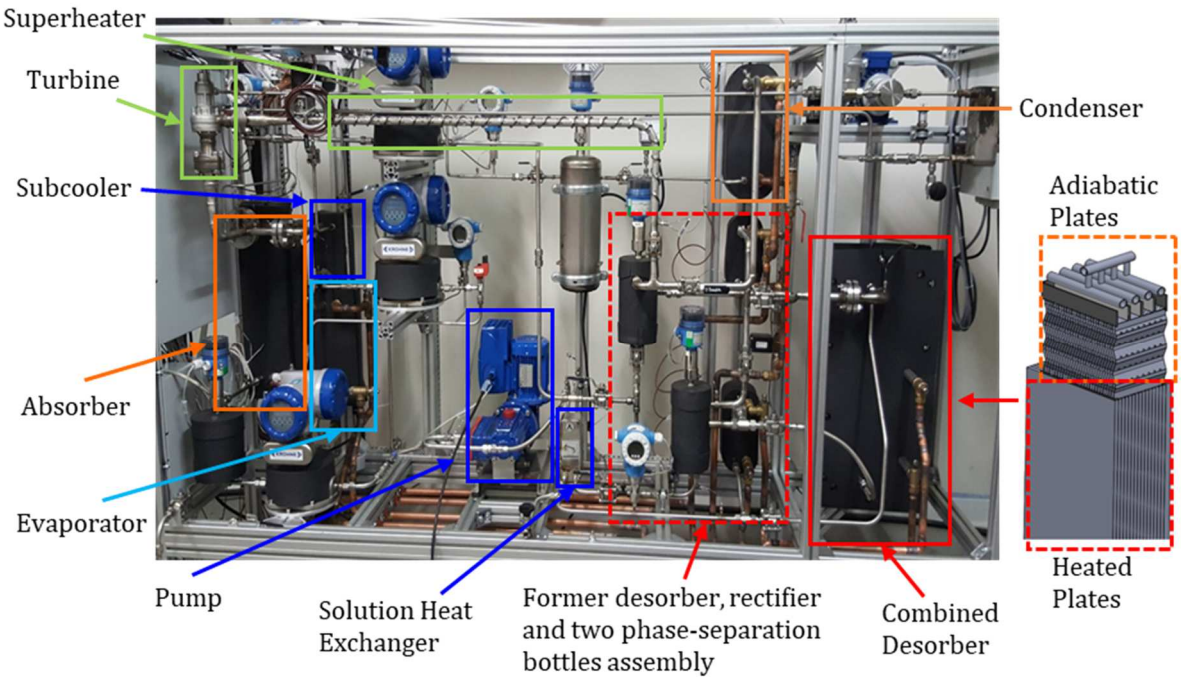

Fig. 2. Picture of the prototype of the NH_3/H_2O combined cycle.

The chiller [17] was originally composed of seven heat exchangers. The five main ones were external heat and mass exchangers: desorber, absorber, evaporator, condenser and rectifier. Among these, the most critical is certainly the absorber, extensively studied and characterised in the absorption chiller prototype by Triché et al. [18]. Two internal heat exchangers, the solution heat exchanger and the subcooler are used to improve the performance of the cycle. Four reservoirs were present in the original absorption chiller: two phase separation tanks (each of 1 L volume) at the outlet of desorber and rectifier, needed to separate the ammonia vapour from water condensate, and two buffer tanks before the pump (0.7 L volume) and subcooler (5.2 L volume). Piping (internal diameter of 10 mm for liquid piping and 17.3 mm for vapour piping) and separation tank design was done in-house to meet operating conditions requirements specific to the prototype.
Usual control components for ammonia-water systems (thermostatic expansion valves, time regulated valves, etc.) could not be found in an adapted size for the prototype [17]. Electronically actuated expansion valves are hence present in the loop, one before the evaporator, regulating the temperature glide during the evaporation process, and the other before the absorber, on the poor solution line, controlling the level of the reservoir upstream of the pump. Volume of the components determines the quantity of water and ammonia needed, which in the case of the prototype are around 1 kg of water and 2.5 kg of ammonia. Filling of the machine is performed by first injecting water in a low point of the prototype close to the reservoir upstream of the pump, and then injecting ammonia in a high point of the machine, near the reservoir downstream the condenser.

Wirtz et al. [19] recently designed and tested a new combined falling-film desorber (**Fig. 3**), performing an internal purification of the desorbed vapour with the rich solution at inlet. This heat exchanger is composed of a distribution system dividing uniformly the rich solution at inlet, a lower part where vapour is generated exchanging heat with the hot source, and an adiabatic upper part allowing the purification of the vapour generated by partial reabsorption of the latter in the ammonia-water solution entering the exchanger. The combination of the heated and adiabatic sections enables replacing two plate heat exchangers used for the desorber and the rectifier as well as two associated phase-separation bottles by only one component, thus helping to reduce costs and overall dimensions.

The high purity of the ammonia vapour at the desorber exit eliminates the need for further purification, making this solution particularly interesting in terms of compactness and performance.
Experimental studies [20] showed that the combined desorber is highly efficient and guarantees very high purity of the ammonia vapour (above 98 % [21]) with a lower heat supply needed compared to a traditional desorber, thus improving the COP of the cycle. Additionally, the functioning of the machine is more stable and steady conditions are reached faster.
The geometry of the desorber as well as that of the other stainless steel corrugated plate heat exchangers is given in **Table 1**

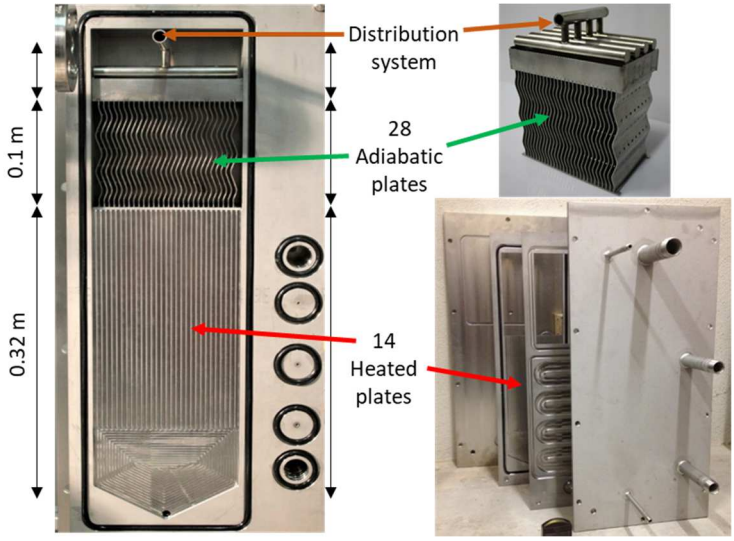

Fig. 3. Exploded view of the combined desorber [19].

Table 1. Dimensions of the heat exchangers of the cycle.

	Absorber	Condenser	Desorber heated (adiabatic) part	Evaporator	Solution Heat Exchanger	Subcooler
Plate width [mm]	96	111	320 (100)	111	72	72
Plate length [mm]	668	310	150 (90)	310	187	187
Plate thickness [mm]	0.5	0.5	6 (0.8)	0.5	0.5	0.5
Number of plates [-]	16	40	16 (28)	24	25	20
Total surface [m^2]	0.89	1.30	0.67 (0.23)	0.75	0.31	0.24

The chiller is connected to a characterization bench, in which independent hydraulic loops fix the temperatures and the mass flow rate of the external heat transfer fluids (HTF) inside the generator, condenser, absorber and evaporator. The temperatures and mass flow rates of HTFs, the rotational speed of the pump (controlling the rich solution mass flow rate) and the opening of the actuated expansions valves (controlling the temperature glide in the evaporator and the level of the buffer tank before the pump) represent the available control parameters. They are used to modify the operating conditions of the chiller to perform the tests necessary for the characterization of the machine. Nominal point and operating range of components are given in **Table 2**.

Table 2. Nominal point and operating range of components.

		Evaporator	Condenser	Absorber	Desorber	Pump
Temperature (inlet/outlet) [°C]	Nominal	18/13	27/32	27/32	95/90	32/33
	Minimal	10/5	22/27	22/27	80/75	-
	Maximal	22/17	30/35	30/35	106/101	50/51
Pressure [bar]	Nominal	7	12	7	12	7/12
	Minimal	5	11	5	11	-
	Maximal	8	14	8	14	5/20
HTF and pump mass flow rate [kg/h]	Nominal	1100	1200	1200	1600	150
	Maximal	1200	1300	1300	1800	250
	Minimal	200	200	200	200	-
Power [kW]	Nominal	7	7	9	10	0.55

3.2. Turbine

Starting from the existing experimental rig described in the previous section, a power production line was added in parallel to the cooling production line. Indeed, part of the pressurised vapour produced at the desorber can be fed to an expander coupled to an electrical generator to produce electricity. Expanders for combined cooling and power cycles benefit from the recent developments of Organic Rankine Cycles (ORC) [22] and are mainly of two types: volumetric or turbomachines. However, since combined production systems are quite complex, only a few experimental investigations have been conducted. Voeltzel et al. [4] proposed the integration of a scroll expander in the testing rig. The model developed by Lemort et al. [23] was adjusted on experimental results from a 1 kW Air Squared scroll expander mounted on an ORC rest rig [16] using R245fa and adapted to use ammonia as a working fluid as detailed by Mendoza et al. [24].
Results highlighted that the leakage area determined for the expander on the ORC rig (5.7 mm^2) would have resulted in quasi-nil production of the scroll in the investigated ammonia-water absorption chiller prototype. Indeed, given the small size of the prototype and the very low mass flow rates (around 20 kg/h), a much higher volumetric efficiency of the expander would have been required (leakage area around 1 mm^2). Additionally, no supplier of scroll expanders working with ammonia was found.
A different power generation technology was therefore investigated for the prototype, that of a turbo-expander. The Balje diagram, illustrated in **Fig. 4**, provides the specific speed N_s and diameter D_s range at the design operation point for each type of turbomachine stage. The selection process requires a preliminary evaluation of N_s and D_s:

$$N_s = \omega \cdot \frac{\sqrt{\dot{m}/\rho_{\text{fluid}}}}{(\Delta h_{is})^{3/4}} \tag{1}$$

$$D_s = D \cdot \frac{(\Delta h_{is})^{1/4}}{\sqrt{\dot{m}/\rho_{\text{fluid}}}} \tag{2}$$

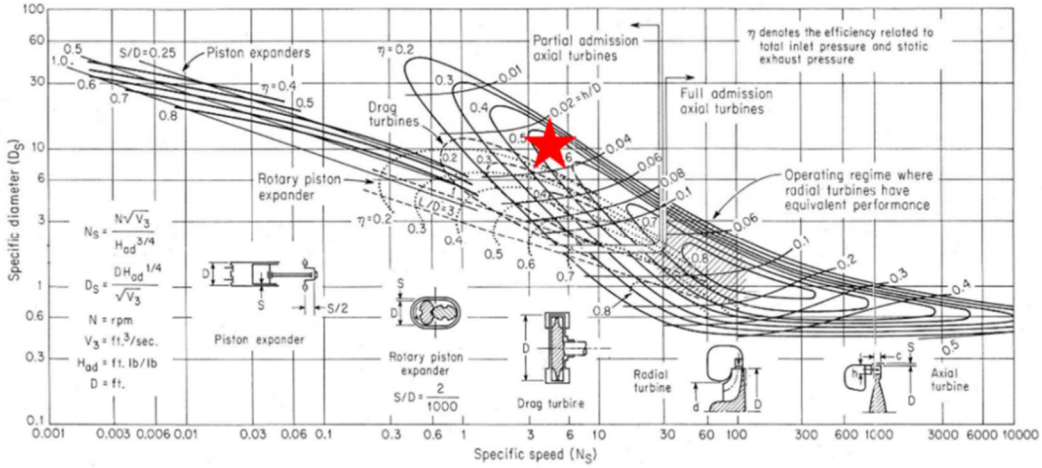

Fig. 4. Balje's N_sD_s *T*urbine chart [25]. The star indicates the calculated turbine working conditions in the prototype.

In this application, the design point considered was: inlet pressure of 16 bar, inlet temperature of 120 °C, outlet pressure of 4 bar, mass flow rate of 20 kg/h. The calculated N_s and D_s of around 2-5 and 10-14 (depending on the different rotational speed and diameter supposed) suggest the partial admission axial turbine to be the best choice (with a total to static maximum efficiency of around 40-50%) [26]. It should be highlighted however that actual conditions achievable in the cycle (**Table 2**) have been later found to be quite different from the supposed designed point of the turbine (16-4 bar) generating important losses during operation.
The expander integrated in the cycle is hence a partial admission supersonic impulse axial turbine, characterised by 27 rotor blades but a distributor composed of a single converging-diverging injector is shown in **Fig. 5**. This choice of expander allows avoiding excessively small and unfeasible dimensions or too high and impracticable rotational speed, at the cost of increased partial admission losses. The diameter of the rotor is of 60 mm, the throat and exit section of the injector are respectively around 2.7 mm^2 and 4.6 mm^2, while the design rotational speed is 75'000 rpm. In addition, the fact that all the expansion takes place in the injector means that there is no pressure drop in the rotor, therefore reducing the performance loss due to leakage, which can represent a substantial disadvantage for machines of this size.
However, despite a design rotational speed of 75'000 rpm, tests performed powering electrically the turbine showed an abrupt increase of vibration for rotational speed above 35'000 rpm, preventing the use of the turbine above 30'000 rpm.

The turbine rotor is made of titanium to reduce its weight and increase the maximum attainable rotational speed, while the rest of the expander is made of stainless steel.
The production of electricity is achieved using a 1950/10 brushless *LMT* electrical motor used as an electrical generator. The output current is three-phase with a variable voltage which is measured by a voltmeter. The electricity produced by the generator is thermally dissipated on an electrical resistance rig composed of 3 electrical resistances (R1=1.2 Ω, R2=2.4 Ω and R3=4.9 Ω respectively) that can be either used individually or arranged in parallel/series to change the total resistance.
The resistance rig allows the expander to evacuate the electricity produced and regulates the rotational speed of the expander which is estimated using the frequency of the electrical power output measured with a frequency meter. Increasing the electrical resistance allows reaching higher rotational speeds.
To increase the efficiency of power production and avoid condensation of the working fluid (of wet type), an electrical superheater of 1kW maximum power is placed before the turbine inlet. Indeed, given the high speed of the flow at the injector outlet, the presence of droplets colliding with the rotor blades could lead to the breaking of the moving parts of the turbine. However, the maximum turbine inlet temperature must be kept below 130 °C, and an additional cooling circuit is installed to keep the temperature of the electrical generator below 60 °C to avoid demagnetization of the permanent magnets of the electric generator.
Finally, the prototype is completed by a line, comprising a variable opening manual valve, allowing to by-pass the turbine to ensure that the vapour conditions are appropriate before allowing its inlet into the turbine. By varying the valve opening, the by-pass line can also be used to assess the impact on the cycle of diverting a variable mass flow rate towards the power production line.

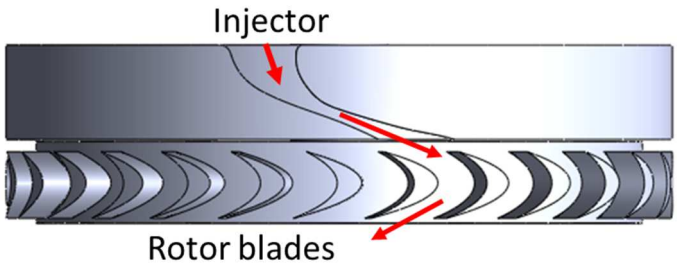

Fig. 5. Schematic diagram of the turbine

3.3. Experimental measurement apparatus

The ammonia-water absorption chiller is fully instrumented (**Fig. 6**) with high precision sensors. Measures of temperature (with T-type thermocouples for working fluid and with a platinum resistance thermometer for heat transfer fluid), density and mass flow rate (with Coriolis flow meters) and pressure are available at the inlet and the outlet of the main components. Liquid level sensors are placed in each reservoir to monitor the fluid distribution in the prototype and, in the case of the reservoir upstream of the pump, ensure safety of operation.
Additionally, the turbine test bench is equipped with measures of tension and frequency, allowing to calculate the rotational speed of the turbine and the electrical power output. The chiller sensors are listed in **Table 3,** where measurement uncertainties refer to the operating range for which sensors have been calibrated.

Table 3. Sensor number and measurement characteristics.

Sensor Type	Number	Uncertainty (±)
P-Type cooling or heating fluid temperature	8	0.50% - 0.13 K
T-type refrigerant and solution temperature	12	0.51% - 0.18 K
Low pressure (0-10 bar)	2	0.48% - 0.03 bar
High pressure (0-20 bar)	2	0.90% - 0.10 bar
Coriolis flow meter	3	0.20% - 0.18 kg/h
Electromagnetic flowmeter	4	0.50% - 0.005 m^3/h
Frequency meter	1	1.7% - 1.7 Hz
Tension	1	0.10% - 0.003V

With this instrumentation, it is possible to calculate both the mass fraction in the different lines of the circuit and formulate energy balances for each component. The power exchanged by each external heat exchanger is calculated through an energy balance on the HTF side knowing the temperature at the inlet and outlet of the exchanger and the HTF mass flow rate. The electrical power produced by the turbine is calculated from the value of voltage and electrical resistance.

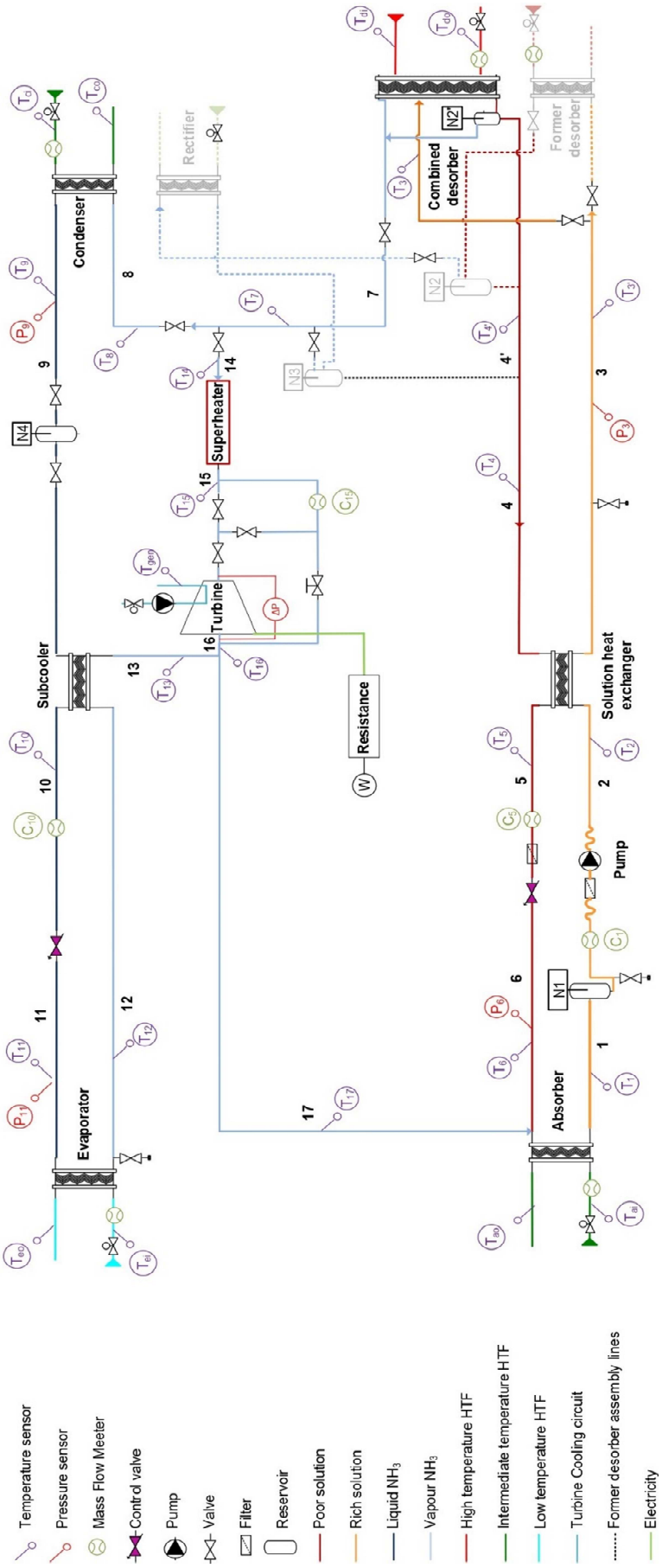

Fig. 6. Schematic view of the machine.

4. Experimental tests

The absorption chiller rig described in **Section 3.1** was tested and characterised in previous investigations, proving to be reliable and capable of achieving good performances. However, several problems were encountered in the combined cycle set-up, not allowing a complete characterisation of the prototype.
A first start-up of the turbine failed due to corrosion problems of the electrical generator. The resin with which the stator coils were initially covered was found to be insufficient in protecting it against the ammonia-water mixture. A re-design of the electricity generation part of the turbine was hence undertaken, leading to the use of a protective casing in titanium separating the rotor and the stator of the electrical generator, protecting it from corrosion. However, the presence of the casing is likely to have greatly reduced the electricity conversion efficiency.
A second start-up of the plant also failed as the turbine stopped functioning in the first hours of tests. The presence of a damaged bearing was revealed by posterior analysis, possibly due to excessive efforts on bearings, highly solicited in partial admission turbines [27]. Indeed, the injection of fluid in an unevenly distributed way causes a radial force on the turbine rotor that, even if below the allowable load of bearings, can increase vibrations. Possible condensation of the working mixture in the absorption cycle loop could increase the already high stress on bearings because of the high velocity of the droplets colliding with the rotor blades. Hence, it was decided to test the turbine outside the loop using nitrogen, argon and compressed air, as presented in *Section 4.1*.
Test performed on the turbine are presented first, followed by tests performed on the combined cycle (*Section 4.2*).

4.1. Turbine

Experimental tests on the turbine alone (state points 14 to 16 in **Fig. 6**) were carried out in order to characterise its functioning. The turbine was tested outside the loop using three different gases (argon, nitrogen and compressed air) and inside the loop with ammonia, using the electrical resistance R1 of 1.2 Ω (see *Section3.2*).Tests outside the loop were performed to enrich the experimental database, since tests with ammonia in the combined cycle rig were not sufficiently numerous and varied. All the tests carried out on the turbine are presented in **Table 4**.
Tests performed with the three gases were performed with a turbine inlet temperature comprised between 20-22 °C, without superheating the vapour. The fluid at outlet was discharged at ambient pressure; however, it was found that increasing the inlet pressure generated a back pressure at the outlet of the turbine, resulting in an outlet pressure between 1.1 and 1.8 bar, depending on the inlet pressure. For this reason, results concerning electricity production, electrical efficiency and rotational speed are presented as a function of the available pressure drop.
The points presented are stationary points (constant inlet pressure and temperature and outlet pressure), averaged over a period of about one minute during which the turbine operating conditions were stable. The measurement uncertainty is estimated to be 0.7% for the mass flow rate and 0.8% for the pressure.

Results in **Fig. 7** show that the mass flow rate treated by the turbine increases linearly with the inlet pressure. This suggests that, in all the conditions tested, the injector was in choking conditions, in which the treated mass flow rate is linearly dependent on the inlet pressure. Indeed, for an ideal gas, the mass flow rate treated by an injector in choking conditions can be written as [28]:

$$\dot{m}_{max} = \frac{P_{in,tot} \cdot A_{throat}}{\sqrt{R \cdot T_{in,tot}}} \cdot \sqrt{\gamma \cdot \left(\frac{2}{\gamma + 1}\right)^{\frac{\gamma+1}{\gamma-1}}} \tag{3}$$

where P is the total pressure in Pa, T is the total temperature in K, A_{throat} is the injector throat section, R is the ideal gas constant $[\mathrm{J/(K \cdot mol)}]$ and γ the gas adiabatic index.

Using **Eq. (3)**, the ideal gas mass flow rate can be calculated for each test point and compared to the experimental mass flow rate as shown in **Fig. 8**. Considering the same injector throat section of 3 mm^2 for all the investigated fluids leads to very good agreements in the case of Argon, Nitrogen and Air, with an average discrepancy of 1.9% and a maximum discrepancy below 5%.
In the case of ammonia, the average discrepancy is above 10%, proving that the use of perfect gas relations in the case of a vapour like ammonia leads to non-negligible errors.

Table 4. Experimental campaign matrix for tests carried out on the turbine.

Test point	Fluid	Electrical resistance [Ω]	P_{in} [bar]	T_{in} [°C]	P_{out} [bar]	$\dot{m}_t$ [kg/h]	Frequency [Hz]	Voltage [VDC]	ω_t [rpm]	$\dot{W}_t$ [W]
1	Argon	1.2	9.98	19.2	2.40	32.0	217	5.88	13071	34.6
2	Argon	1.2	8.94	18.2	2.17	28.6	203	5.36	12200	28.7
3	Argon	1.2	8.03	17.8	1.94	25.6	193	5.00	11599	25.1
4	Argon	1.2	7.11	17.6	1.71	22.4	180	4.65	10831	21.6
5	Argon	1.2	6.02	17.6	1.50	18.8	155	3.75	9330	14.1
6	Argon	1.2	5.03	17.6	1.36	15.5	129	2.93	7780	8.6
7	Argon	1.2	4.04	17.8	1.24	12.3	109	2.24	6565	5.0
8	Argon	1.2	3.02	17.9	1.14	9.1	84	1.40	5081	2.0
9	Nitrogen	1.2	9.24	17.8	2.20	23.4	223	6.08	13405	37.0
10	Nitrogen	1.2	7.06	16.9	1.68	17.6	192	4.94	11522	24.4
11	Nitrogen	1.2	5.84	16.7	1.45	14.5	162	3.94	9732	15.6
12	Nitrogen	1.2	5.02	16.7	1.34	12.3	134	3.04	8058	9.2
13	Nitrogen	1.2	3.69	16.8	1.18	8.9	101	2.00	6111	4.0
14	Air	1.2	3.04	21.7	1.14	7.3	83	1.37	5008	1.6
15	Air	1.2	4.02	22.2	1.23	9.8	108	2.17	6484	3.9
16	Air	1.2	5.0	22.5	1.3	12.4	133	3.0	8021	7.5
17	Air	1.2	7.11	23.2	1.74	17.9	188	4.87	11333	19.8
18	Air	1.2	7.82	23.7	1.90	19.8	203	5.30	12186	23.4
19	Air	1.2	7.08	23.5	1.72	17.8	190	4.93	11415	20.3
20	Air	1.2	6.04	23.3	1.49	15.1	166	4.16	10006	14.4
21	Air	1.2	5.04	23.1	1.34	12.4	137	3.20	8275	8.5
22	Air	1.2	4.01	22.7	1.23	9.8	103	2.02	6230	3.4
23	Air	1.2	6.94	22.0	1.76	18.0	156	4.48	9373	16.7
24	Air	1.2	6.04	21.8	1.55	15.5	139	3.83	8359	12.2
25	Air	1.2	5.04	21.6	1.38	12.8	117	3.03	7029	7.6
26	Air	1.2	4.04	21.4	1.25	10.1	94	2.13	5674	3.8
27	Air	1.2	3.03	21.2	1.16	7.4	72	1.33	4374	1.5
28	Air	2.4	6.99	22.0	1.78	18.2	243	8.06	14633	27.0
29	Air	2.4	6.02	21.6	1.55	15.5	216	7.00	12976	20.4
30	Air	2.4	5.05	21.5	1.39	12.8	178	5.54	10712	12.8
31	Air	2.4	4.04	21.2	1.26	10.1	139	4.06	8386	6.9
32	Air	2.4	3.05	21.0	1.16	7.5	101	2.53	6080	2.7
33	Air	5.9	7.05	22.1	1.75	na	372	13.44	22363	36.9
34	Air	5.9	6.05	21.9	1.52	na	324	11.46	19471	26.8
35	Air	5.9	5.1	21.5	1.3	na	264	9.0	15895	16.7
36	Air	5.9	4.05	21.1	1.22	na	204	6.67	12290	9.1
37	Air	5.9	3.04	21.0	1.12	na	142	4.20	8561	3.6
38	Air	5.9	2.05	20.7	1.06	na	78	1.74	4726	0.6
39	Air	8.2	6.82	22.6	1.71	na	445	16.42	26746	32.9
40	Air	8.2	6.04	22.4	1.53	na	400	14.57	24038	25.9
41	Air	8.2	5.0	22.0	1.4	na	332	11.9	19921	17.1
42	Air	8.2	4.04	21.7	1.23	na	258	8.90	15489	9.7
43	Air	8.2	3.03	21.4	1.14	na	178	5.68	10721	3.9
44	Air	8.2	2.02	21.1	1.07	na	91	2.29	5513	0.6
45	Ammonia	1.2	12.02	94.1	5.15	20.5	0	5.31	na	23.5
46	Ammonia	1.2	12.29	98.7	5.41	20.7	0	5.60	na	26.1
47	Ammonia	1.2	11.53	102.3	5.32	19.2	0	5.65	na	26.6
48	Ammonia	1.2	11.48	102.7	5.19	19.1	184	5.47	11016	24.9
49	Ammonia	1.2	11.53	100.8	5.10	19.2	179	5.33	10730	23.7
50	Ammonia	1.2	11.31	98.0	4.65	18.6	175	4.85	10516	19.6
51	Ammonia	1.2	11.31	95.1	4.66	19.3	161	4.80	9640	19.2
52	Ammonia	1.2	11.36	96.9	4.74	19.0	154	na	9261	na
53	Ammonia	1.2	11.25	99.2	4.97	19.1	0	na	na	na
54	Ammonia	1.2	11.77	99.3	5.11	20.0	0	na	na	na
55	Ammonia	1.2	11.91	99.0	5.11	20.2	0	na	na	na
56	Ammonia	1.2	12.01	98.2	5.11	20.4	0	na	na	na
57	Ammonia	1.2	12.18	98.2	5.03	20.7	0	na	na	na
58	Ammonia	1.2	12.44	97.4	4.71	21.1	0	na	na	na
59	Ammonia	1.2	10.97	100.0	4.71	18.5	0	na	na	na
60	Ammonia	1.2	11.50	97.0	4.58	19.4	0	na	na	na
61	Ammonia	1.2	10.90	90.6	3.61	24.2	0	na	na	na
62	Ammonia	1.2	11.75	93.7	5.09	20.1	0	na	na	na

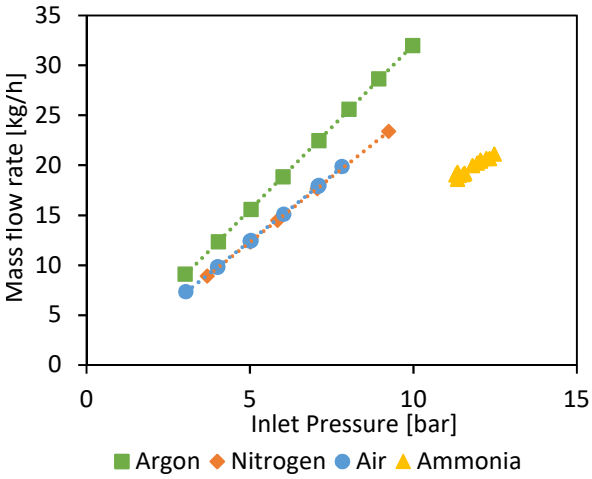

Fig. 7. Treated mass flow rate as a function of the inlet pressure.

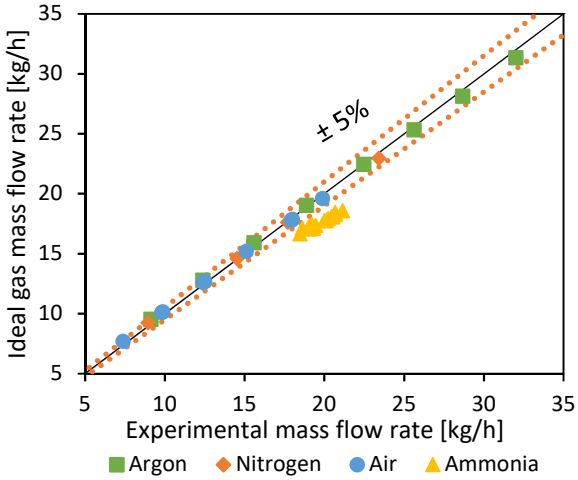

Fig. 8. Experimental vs ideal gas turbine mass flow rate.

Fig. 9 shows that, as expected, when the available pressure drop on the turbine increases, the electrical power produced by the turbine also increases. In particular, the power output increases slightly more than linearly due to the combined effect of the increasing mass flow rate and of the increasing efficiency at higher rotational speed. The measurement error on the electrical power produced is estimated below 1%, while the error in measuring the rotational speed is estimated at 1.7%.

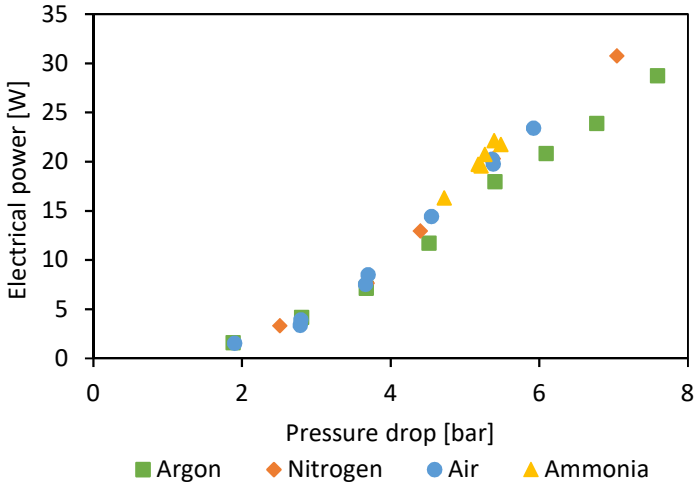

Fig. 9. Electrical power of the turbine as a function of the pressure drop using R1=1.2 Ω.

As mentioned above, the electrical power output increase also depends on the electrical efficiency increase. Increasing the pressure drop on the turbine also increases its rotational speed, as shown in **Fig. 10(b)**, thus bringing the turbine closer to its optimal operating point, and increasing its electrical efficiency (**Fig. 10(a)**), defined as [29]:

$$\eta_{el} = \frac{\dot{W}_{el}}{\dot{W}_{is}} \tag{4}$$

Where $\dot{W}_{is}$ is defined as: $\dot{W}_{is} = \dot{m} \cdot [h(P_{in}, T_{in}) - h(P_{out}, s_{in})]$.

As shown in **Fig. 9** and **Fig. 10**. The electrical power output and efficiency of the turbine are much lower than expected. This is due to several factors, including shocks taking place during the expansion, the low efficiency of the electrical generator (generally below 50-60% for these power range [29], but here certainly much lower), the additional losses generated by the titanium casing protecting the coils and the low rotational speeds reached.

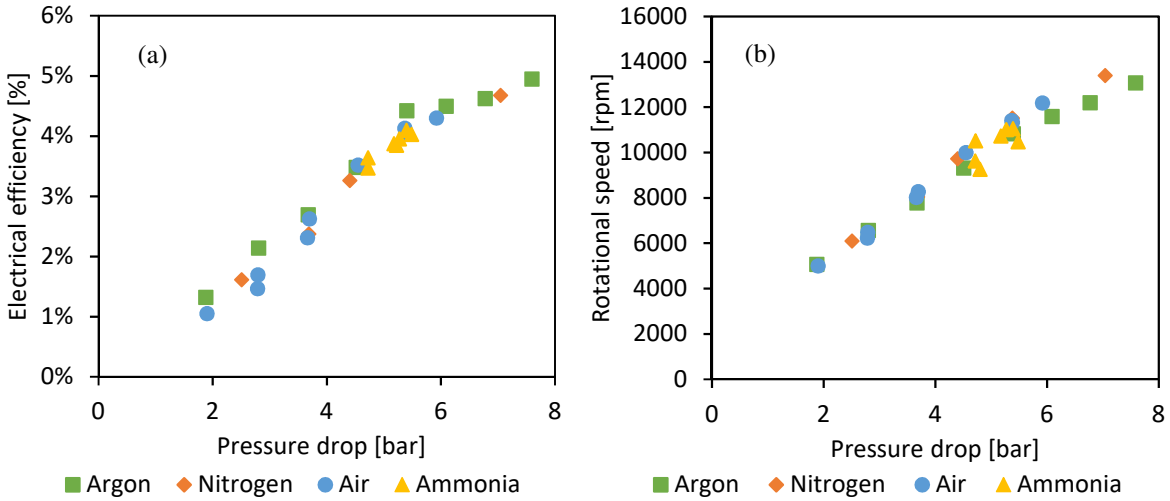

Fig. 10. Electrical efficiency and rotational speed increase as a function of the pressure drop using R1= 1.2 Ω.

To assess the influence the of the rotational speed on the turbine performance, additional tests were carried out using compressed air and changing the value of the electrical resistance. For a given pressure drop, increasing the electrical resistance results in higher rotational speeds of the turbine, as presented in **Fig. 11**.

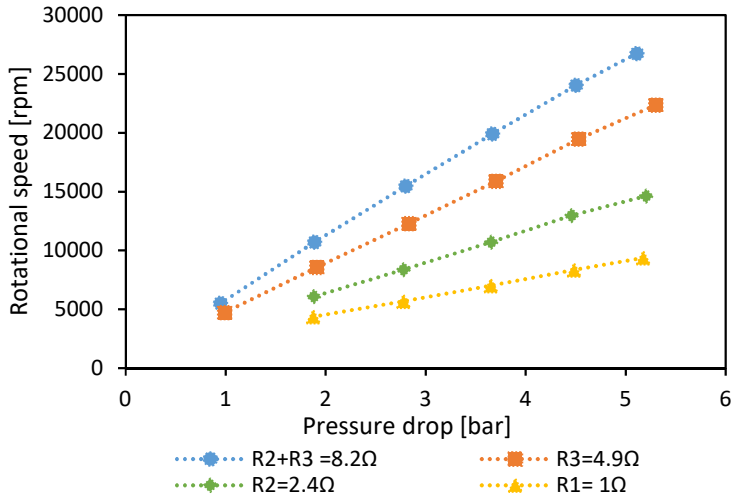

Fig. 11. Rotational speed of the turbine as a function of the pressure drop for different values of the electrical resistance and air as a working fluid.

On the other hand, increasing the pressure drop initially increases the electrical efficiency (**Fig. 12(a)**) and the electrical power output (**Fig. 12 (b)**) of the turbine, but in the case of compressed air, it seems that a maximum is reached between 4.9 and 8.2 Ω.

Calculating by interpolation the values of rotational speed, electrical power and electrical efficiency from **Fig. 11** and **Fig. 12**, for different values of the pressure drop, it is possible to find the electrical power output and electrical efficiency characteristic of the turbine. The result are the bell-shaped curves typical of axial turbines [28], shown in **Fig. 13**, in which each point represents the use of a different electrical resistance. As expected, the power output and the electrical efficiency of the turbine increase when the pressure drop increases, reaching a maximum around 33 W and an electrical efficiency of 7% for a rotational speed of around 20'000 rpm when the available pressure drop is 5 bar. Additionally, the optimal working point shifts at higher rotational speeds when the pressure drop is increased.

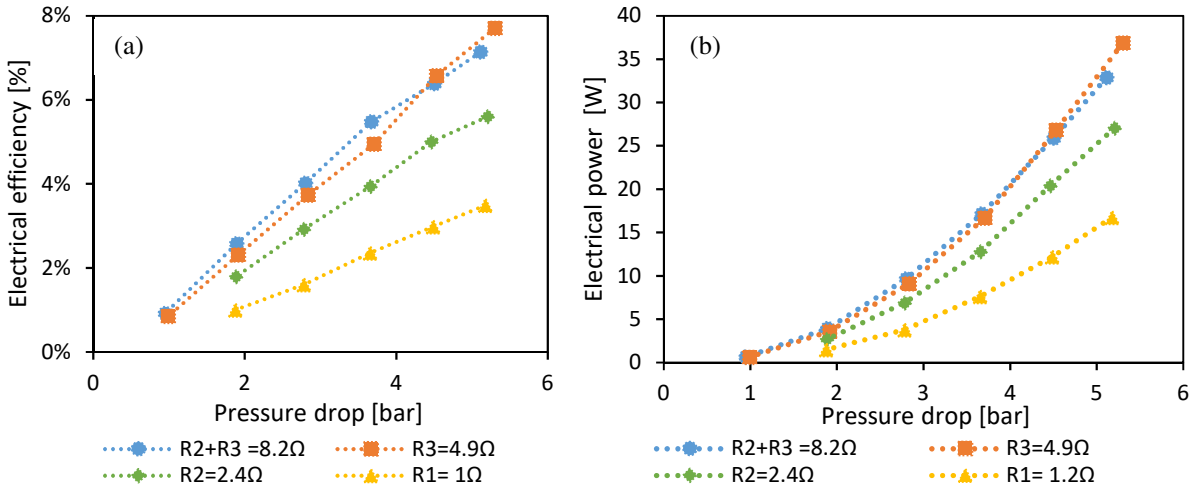

Fig. 12. Electrical efficiency (a) and electrical power output (b) of the turbine as a function of the pressure drop for different values of the electrical resistance and air as working fluid.

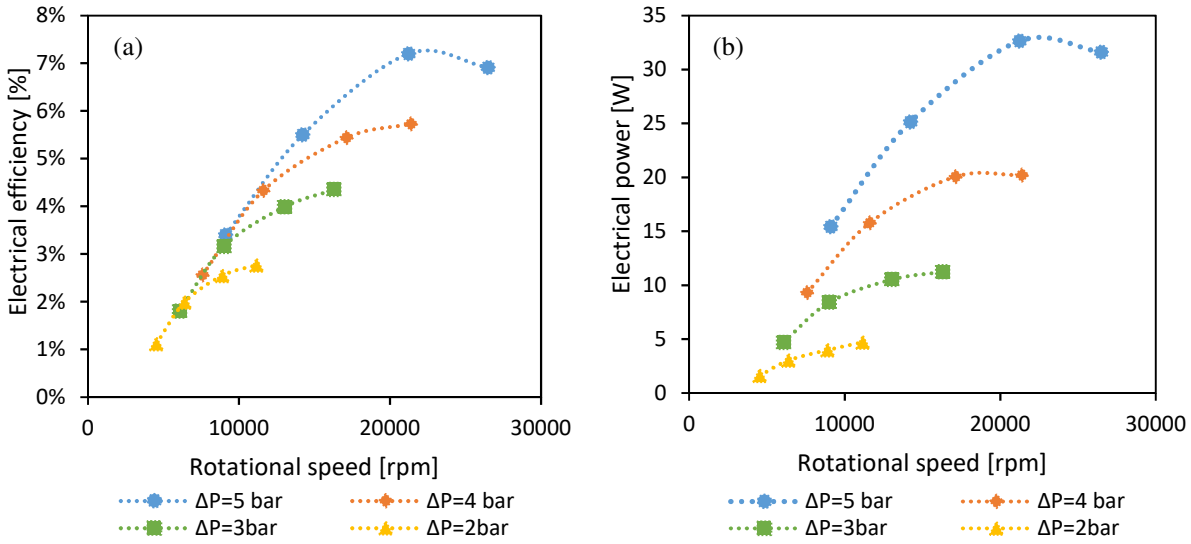

Fig. 13. Electrical power output (a) and electrical efficiency (b) of the turbine as a function of the rotational speed for different values of the available pressure drop (using air as working fluid).

Finally, the influence of the turbine inlet temperature was evaluated in the case of compressed air. Impulse turbines like the one investigated here transform a pressure difference into an increase of the velocity of the flow [26]. Therefore, inlet and outlet pressures represent the most important variables, while temperature-related effects are of secondary importance [26]. This is shown in **Fig. 14** referring to the use of resistance R2 (4.9 Ω), where two different inlet temperatures, 70 °C and 20 °C, are compared. Increasing the turbine inlet temperature has a negligible effect on the electrical power output. The isentropic enthalpy drop increases, passing from 96 kJ/kg for an inlet at 20 °C to 112 kJ/kg for an inlet temperature of 70 °C (inlet pressure 7 bar, outlet pressure 1.75 bar). However, this is almost completely compensated by a reduction of the turbine mass flow rate passing from 18.5 kg/h at 20 °C to 17.5 kg/h at 70 °C, due to the lower density of the working fluid at higher temperatures.

In conclusion, tests performed on the turbine showed that in all the points tested the expander was in choking conditions. Therefore, a linear dependency reported between the turbine inlet pressure and the treated mass flow rate is in accordance with theory [30]. The real-gas assumption leads to relevant errors for the turbine mass flow rate calculation in the case of ammonia, while discrepancies are negligible for the other tested gases. The overall electrical efficiency and power production are strongly correlated to the pressure drop across the turbine and its rotational speed for all fluids tested. Finally, the turbine inlet temperature has a limited influence on the turbine electrical efficiency.

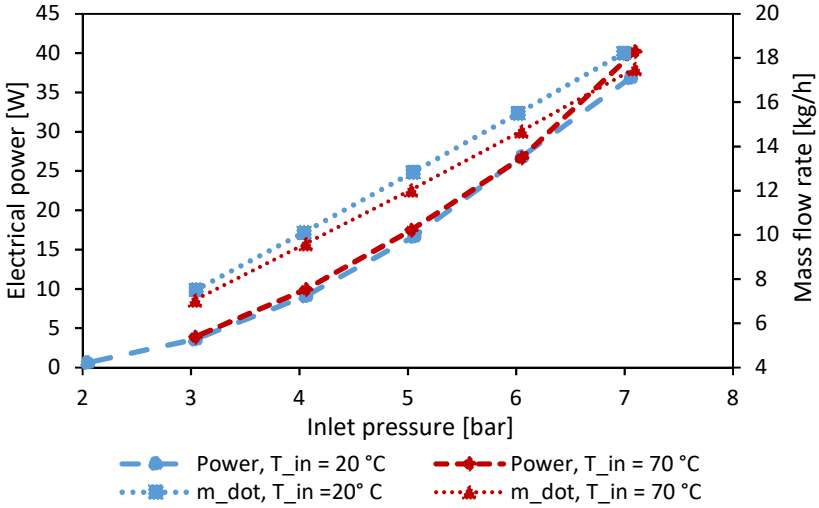

Fig. 14. Electrical power output and turbine mass flow rate as a function of the turbine inlet pressure for 2 different temperatures using the resistance R3= 4.9 Ω (using air as working fluid).

4.2. Combined cycle

The turbine was integrated in the absorption chiller prototype to evaluate the interaction between this expander and the cycle. Tests performed are listed in **Table 5**, where ABS mode indicates that the machine was working in simple absorption working mode, i.e. split ratio (defined as $r_s = \dot{m}_8/\dot{m}_7$ with reference to **Fig. 1**) $r_s = 1$. ACP indicates the combined cooling and power working mode and PC indicates the power cycle working mode in which only the turbine line is open, i.e., $r_s = 0$.

Table 5. Combined cooling and power production prototype experimental campaign matrix. Points marked with an asterisk represent test points performed after the dysfunctioning of the turbine.

Point	Mode	T_{di} [°C]	T_{ai} [°C]	T_{ei} [°C]	T_{15} [°C]	$\dot{m}_{10}$ [kg/h]	$\dot{m}_{15}$ [kg/h]	r_s [-]	P_3 [bar]	P_{11} [bar]	$\dot{Q}_d$ [kW]	$\dot{Q}_e$ [kW]	$\dot{W}_t$ [W]	COP [-]
1	ABS	82.8	27.2	17.8	14.5	14.7	0	1.00	11.74	5.83	7.6	4.5	na	0.58
2	ABS	102.7	27.6	17.8	27.4	16.1	0	1.00	12.06	6.34	9.9	4.9	na	0.49
3	ACP	102.3	29.0	17.6	94.1	10.6	20.5	0.34	12.02	6.87	13.7	2.1	23.5	0.44
4	ACP	104.8	29.8	17.8	98.7	10.9	20.7	0.35	12.29	6.87	14.1	2.2	26.1	0.45
5	ACP	104.6	27.0	17.8	102.3	12.0	19.2	0.38	11.53	6.20	14.1	3.7	26.6	0.69
6	ACP	105.4	27.2	17.9	102.7	10.5	19.1	0.35	11.48	6.29	13.5	3.2	24.9	0.67
7	ACP	100.2	27.4	17.9	100.8	10.2	19.2	0.35	11.53	6.42	13.0	3.0	23.7	0.67
8	ACP	94.1	26.8	17.9	98.0	10.2	18.6	0.36	11.31	6.66	12.3	3.0	19.6	0.69
9	ACP	94.1	26.9	17.8	95.1	10.5	19.3	0.35	11.31	6.66	12.9	3.1	19.2	0.68
10	ACP*	94.1	27.0	17.8	96.9	10.6	19.0	0.36	11.36	6.62	12.7	3.1	na	0.68
11	ABS*	94.1	27.6	17.9	39.7	22.0	0	1.00	12.46	5.97	10.1	6.6	na	0.66
12	ACP*	100.3	26.2	17.7	99.2	11.4	19.1	0.37	11.25	6.29	13.7	3.6	na	0.70
13	ACP*	100.3	28.3	17.7	99.3	10.3	20.0	0.34	11.77	6.67	13.4	2.9	na	0.64
14	ACP*	100.2	28.9	17.8	99.0	10.0	20.2	0.33	11.91	6.81	13.4	2.7	na	0.60
15	ACP*	100.3	29.4	17.8	98.2	9.9	20.4	0.33	12.01	6.90	13.3	2.4	na	0.55
16	ACP*	100.2	30.6	17.8	98.2	9.8	20.7	0.32	12.18	7.15	13.3	1.7	na	0.39
17	ACP*	100.2	33.2	18.4	97.4	9.7	21.1	0.31	12.44	7.73	13.3	0.5	na	0.12
18	ACP*	100.2	26.6	14.8	100.0	12.5	18.5	0.40	10.97	6.27	13.5	2.2	na	0.41
19	ACP*	100.1	28.2	17.7	97.0	12.8	19.4	0.40	11.50	6.92	13.8	2.1	na	0.39
20	PC*	89.2	27.0	17.8	90.6	0.0	24.2	0.00	13.83	7.29	10.6	0.0	na	0.00
21	ACP*	99.1	28.3	17.7	93.7	10.1	20.1	0.33	11.75	6.66	13.2	2.9	na	0.66

The last column of **Table 5** reports the cooling COP of the cycle defined as $COP_c = \dot{Q}_e/(\dot{Q}_d \cdot r_s)$ where, to account for the fact that not all the refrigerant vapour is used for the cooling production, $\dot{Q}_d$ is multiplied by the split ratio r_s . The COP_c is merely a partial performance parameter characterising the cooling line efficiency, while exergy efficiency would be a meaningful overall performance metrics for such combined cycle [31]. However, the use of a second principle performance parameter for the pilot plant under investigation would not have resulted in

generalizable conclusions, as it would be excessively affected by the small size and extreme partial admission rate of the turbine, leading to extremely low isentropic efficiency of the expander, while on the other hand, the cooling production efficiency is not equally affected by the small size. Hence, the COP_c is reported in **Table 5** for the reader's reference, while more details about exergy efficiency of such cycle is given in [31].
Test points marked with an asterisk (point 10-21) represent tests performed after the breaking of the turbine as explained in *Section 4*. Although the turbine had stopped rotating, given the very small power extracted from the fluid by the turbine, these points give interesting insights on the effect of diverting a part of the desorbed vapour mass flow rate to the turbine line. As in the case of the tests performed on the absorption cycle, also in this case the temperature glide in the evaporator was fixed to 5 °C for all points.

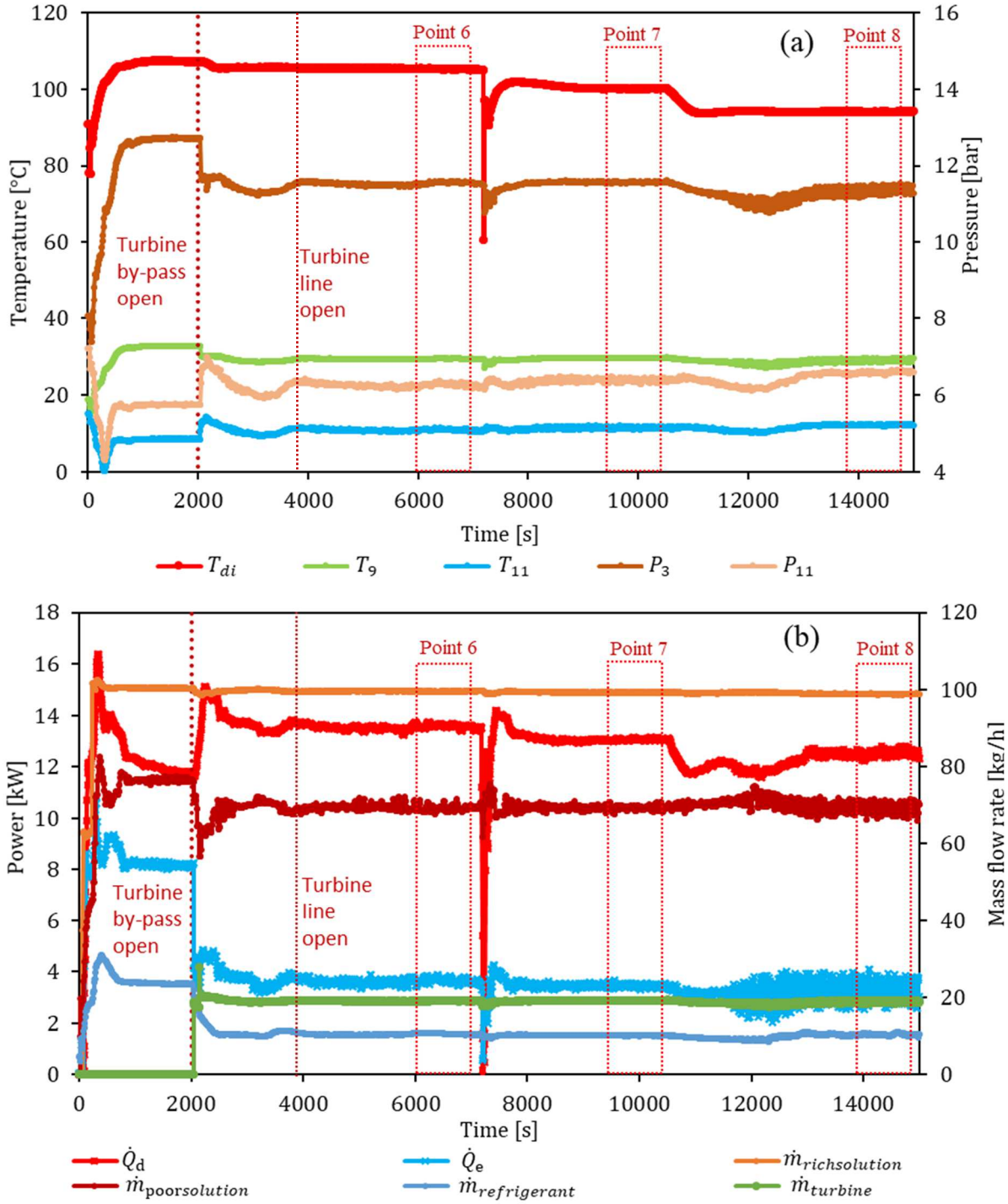

Fig. 15. Impact of the desorber temperature variation (T_{ai}= 27 °C, T_{ei}= 18 °C).

The effect of changing the desorber temperature, all other conditions kept constant, is shown in **Fig. 15** (corresponding to points 6-8 in **Table 5**), referring to an intermediate source temperature of 27 °C, a cold source temperature of 18 °C and a solution mass flow rate of 100 kg/h. In these tests, the cycle is initially started in the simple absorption operating mode. The external networks are started first, and once the temperature set point is approached, the cycle is started in the initialisation mode. During this 3-minute phase, the pump is started up at a reduced speed, circulating around 60 kg/h of rich solution. After that phase, the time required to reach stable conditions is less than 15 minutes (900 s). Once stable conditions are reached, the turbine by-pass valve is opened and the superheater is started to reach the desired turbine inlet temperature before opening the valve upstream of the turbine and closing the by-pass valve. This protocol was used as an initial precaution to ensure adequate turbine inlet conditions in terms of vapour quality and temperature, in particular to avoid condensation during expansion.

Switching from the simple absorption to the combined cooling and power working mode deviates part of the vapour mass flow rate to the power production line. Consequently, passing to a combined production working mode reduces the high pressure of the cycle, while it increases the low pressure. Indeed, for the condenser a smaller mass flow rate results in a lower temperature of the fluid at the condenser outlet (T_9), hence reducing the high pressure of the cycle, fixed by the condenser. For the evaporator instead, the temperature pinch with the cold source is reduced and hence the temperature at the evaporator inlet (T_{11}) increases, increasing the low pressure of the cycle, as shown in **Fig. 15(a)**. Since the absorption process is favoured by a higher pressure, and desorption by a lower pressure, this results in an increase in the circulating vapour mass flow rate as shown in **Fig. 15(b)**.

The variation of the desorber temperature (point 6-8) seems to have little impact on the working pressure and mass flow rates of the cycle. Indeed, while the power absorbed from the hot source decreases when reducing its temperature, the cooling power as well as the mass flow rate passing through the turbine remain almost unchanged, indicating the efficiency of the cycle increases (for T_{ai} = 27 °C, T_{ei} = 18 °C). However, the functioning of the cycle becomes unstable and it is difficult to operate the plant with a hot source below 95°C. It should be noted that the peaks seen in **Fig. 15** are determined by the PID control of the hot source temperature and not by the operating characteristics of the machine.
The influence of the intermediate source temperature T_{ai} is presented in **Fig. 16** (corresponding to points 12-17 in **Table 5**). A reduction of the cooling power output when the intermediate source temperature increases can be seen, in accordance with the theory on absorption machines functioning [2]. However, while increasing T_{ai} reduces the efficiency of the cooling production cycle, it also increases the high pressure of the cycle (**Table 5**), passing from 11.25 bar for T_{ai} =26.2 °C to 12.44 bar for T_{ai}=33.2 °C. This is favourable for the turbine, which can benefit from a higher ΔP and a higher mass flow rate (linearly dependent on the inlet pressure, as shown in **Eq. (3)**) and thus conclusions drawn in the previous section show that its power output increases. However, the high pressure of the cycle increases less than linearly when increasing T_{ai}, mitigating the positive effect on the power production. Indeed, since a higher mass flow rate is deviated to the power production line, the temperature pinch on the condenser is reduced with an effect on the cycle high pressure.
Similar considerations apply for a variation of the cold source temperature T_{ei}. Lowering this temperature reduces the cooling production output but increases the ΔP available to the turbine.

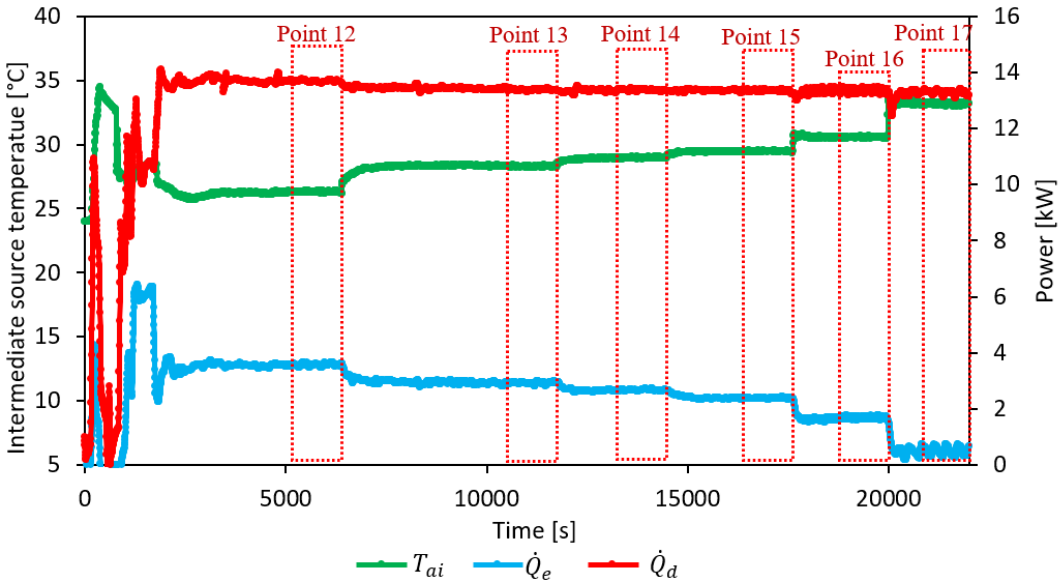

Fig. 16. Intermediate source temperature variation (T_{di} = 100 °C, T_{ei} = 18 °C, $\dot{m}_1$ =100 kg/h).

Fig. 17 shows the transition from a stable point with the turbine line closed to a stable point with the turbine line open. After the turbine line opening (at t=2300 s) the time required to reach stable functioning is below 180 s (3 minutes), but it can be notices that the turbine reaches stable functioning more quickly.
The same considerations discussed before apply to the increase in the circulating vapour mass flow rate and the variation of the working pressures when part of the circulating vapour is deviated towards the turbine. Additionally, since the power absorbed by the hot source increases from 9.9 kW to 13.7 kW, it is difficult for the intermediate temperature HTF modules to reject all the power absorbed from the cycle. Hence, the absorber and condenser HTF inlet temperature increases from the set point of 27 °C to around 29 °C. Moreover, the sudden decrease of poor solution mass flow rate that takes place at the opening of the turbine line indicates that the desorber is probably capable of producing all the vapour requested, but the absorber then becomes limiting and causes the circulating vapour mass flow rate to stabilise at a lower value.

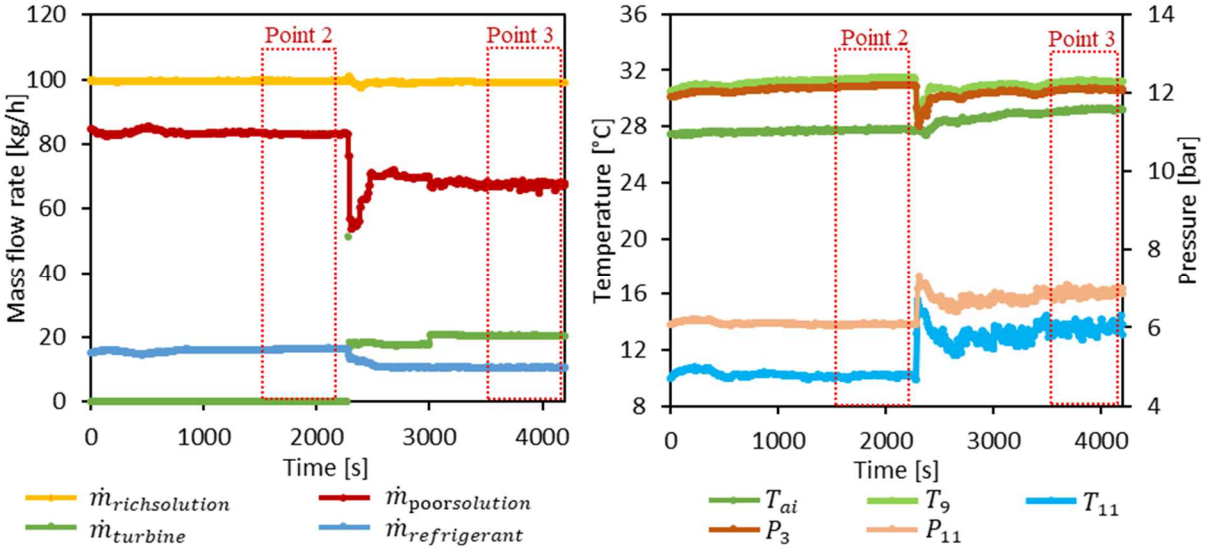

Fig. 17. Working mode switching from simple absorption to absorption cooling and power (T_{di} = 102 °C, T_{ai} = 18 °C).

The opposite mode switch is shown in **Fig. 18.** Here passing from a combined production mode to a simple absorption mode decreases the mass flow rate of circulating vapour, increases the high pressure of the cycle and decreases the low pressure. In this case, since the desorber inlet temperature (94°C) is lower than in the previous case shown in **Fig. 17** (102 °C), the power absorbed from the hot source is smaller. Hence, the power to be rejected to the intermediate source is also smaller and it is possible to maintain the set intermediate source temperature of 27 °C also in the combined production working mode.

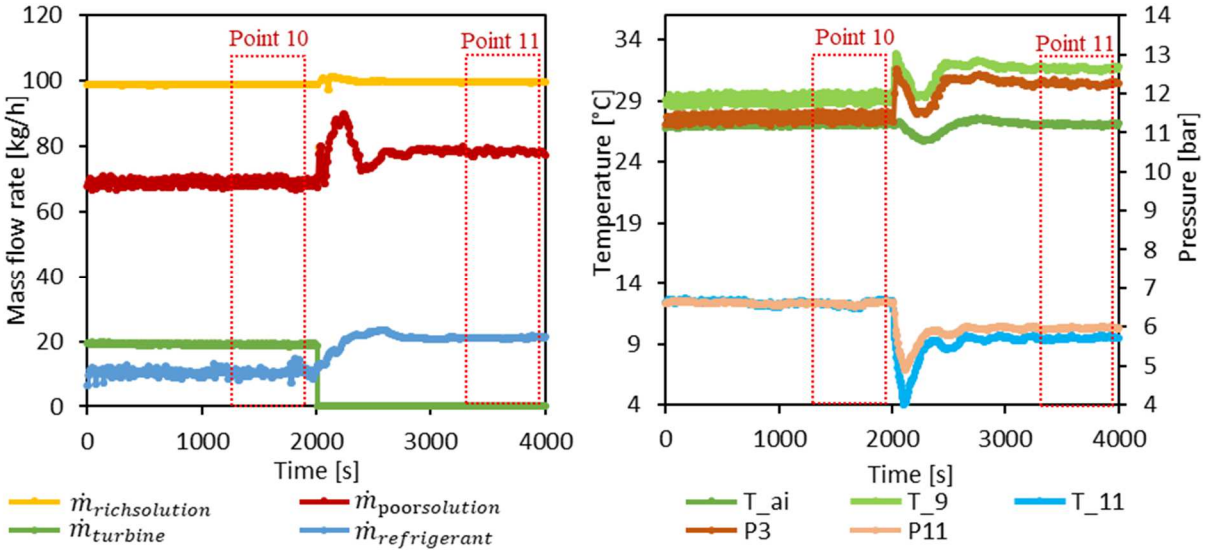

Fig. 18. Working mode switching from absorption cooling and power to simple absorption (T_{di} = 94 °C, T_{ei} = 18 °C).

In general, as in the case of the absorption chiller working mode, the dependency of the working pressures from the condenser outlet and evaporator inlet temperatures remains also in the combined production working mode. Additionally, the functioning is more unstable in the combined production working mode.
Functioning as power cycle (equivalent to a Kalina cycle) was also tested. In this operating mode, the high pressure of the cycle is defined by an equilibrium between the mass flow rate that can be treated by the turbine at a given pressure and the amount of steam desorbed at the same pressure. The low pressure of the cycle is instead fixed by the absorption temperature (of the intermediate temperature source), which in this case takes place in the absorber. In the case of the prototype, the safeties are set to stop the loop if a pressure of 14 bar is exceeded. Hence, stable functioning as a power cycle was only possible for low temperatures of the hot source (below 90 °C).
Starting and stopping the system were tested in all three possible working modes showing that the plant is flexible enough to be started or stopped in any configuration, provided that adequate operating conditions are imposed.
Finally, tests to assess the effect of diverting an increasing part of the vapour mass flow rate to the power production line were carried out. Since this was not possible using the turbine, tests with variable opening of the turbine by-pass valve were conducted. Results, shown in **Fig. 19**, show that increasing the valve opening increases the mass flow rate of desorbed refrigerant vapour (passing from around 20 kg/h when the valve is closed to almost 30 kg/h when it is fully open).

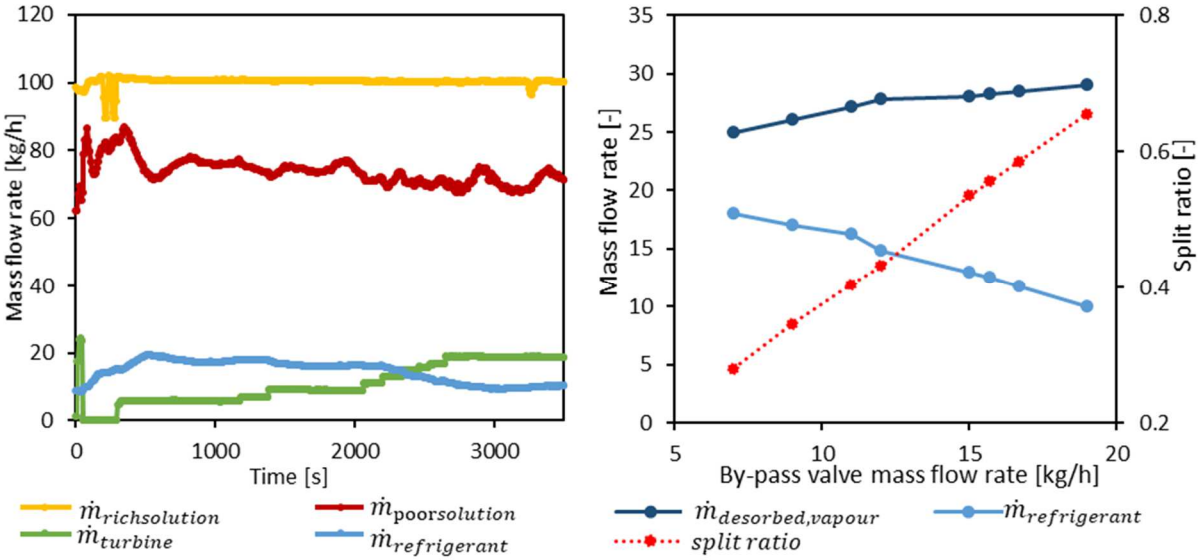

Fig. 19. Variation of the turbine by-pass valve opening (T_{di} = 100 °C, T_{ai} =18 °C, T_{ei} =18 °C, $\dot{m}_1$ =100 kg/h).

In conclusion, the integration of the micro-turbine into the single-stage absorption chiller plant has been analysed through an experimental campaign. Tests were conducted only around the nominal operating point of the absorption chiller due to limitations of the test bench. Dynamic switching between the three possible operating modes was tested and proved to be stable and quick to reach steady state. One of the main findings of these tests is that the lack of possibility to regulate the mass flow rate treated by turbine imposes strict limits on the cooling production side of the loop.
Moreover, the reduced mass flow rate passing through the cooling side heat exchangers (condenser and evaporator) increases their efficiency, affecting the pressures equilibrium established within the cycle and the circulating vapour mass flow rate.

4.3. Feedback from experimental tests on the prototype

The experimental tests performed on the pilot plant allowed a deeper understanding of the system's operation, its operating range and its limitations.
A first limitation worth mentioning is that the bench was designed for a cold source temperature of 18 °C (resulting in cooling production at around 13-15 C°) and performance of the system decreases considerably at lower temperature. Also, since the HTF used is water, the cold production temperature would in any case be limited to positive temperatures.

Aspects to be given great attention are the operation of the electronically actuated valves and the level control in the tanks. Wearing of valves could lead to instabilities in the machine's operation and strongly fluctuating behaviour. The expansion valve on the poor solution line for example needed to be replaced twice during testing. This valve, in addition to ensuring the pressure drop necessary for the functioning of the cycle, is also in charge of controlling the liquid level in the tank before the pump. This parameter also proved to be important and influential on the operational stability of the system, as it regulates the quantity of working fluid circulating in the loop. Experience on the pilot plant suggests that this level should be regulated to 60 mm when using the combined desorber/rectifier.

Another important issue is the flooding of the desorber. As previously stated, Wirtz [19] characterised the desorber both in the unflooded and partially flooded working mode. However, the flooding of the desorber is not desirable, but rather an issue due to problems of design and positioning of the component in the loop. Avoiding flooding of the desorber can be rather challenging and specific operating protocols need to be used. Wirtz [19] reported that setting the desorber temperature initially at a higher value and then lowering it to the desired value appeared to be an effective way to avoid flooding of the desorber.
One last point concerns the choice of the temperature glide in the evaporator. When the ammonia vapour purity is not high, the temperature glide in the evaporator can be considerable [2]. This glide can be reduced by allowing some liquid at the evaporator exit, which is then evaporated in the subcooler. However, the presence of the liquid degrades the cycle performance because energy is spent in the desorber to produce vapour which provides no refrigeration [2]. On the other hand, an excessive temperature glide leads to a reduction of the evaporator inlet temperature, with a strong impact on the pressures and performance of the cycle. The choice of this parameter can then have a strong impact on the performance of the cycle. In the experimental prototype, it is set (generally at 5 °C) by regulating the mass flow rate on the cooling production line through the actuated throttling valve placed before the evaporator.

In the case of the turbine, an improper definition of the design point (inlet pressure of 16 bar and outlet pressure of 4 bar) leads to the presence of shocks and non-isentropic adjustment phenomena when the turbine is used in the cycle (with an inlet pressure usually below 12 bar and an outlet pressure usually above 6 bar). In addition, a very low efficiency of the electricity generation (further degraded by the titanium casing protecting the coils), very low achievable rotational speeds and important mechanical losses result in extremely low values of electricity production of the turbine. Worth mentioning are also the difficulties of controlling the turbine inlet temperature using the electric superheater. Finally, the problem of the condensation of the working mixture during expansion remains to be investigated.

Concerning the combined cycle, the most important limitations highlighted concern the limited operating range of the bench. Indeed, there is a limit to the total power that can be exchanged by external circuits, which in total cannot exceed approximately 40 kW. Because of this, it is not possible to achieve desorber temperatures beyond 110 °C-115 °C. Furthermore, the maximum cycle pressure is limited to 14 bar, which did not allow the machine to be characterised in detail in the power cycle working mode. Lastly, the strict limits imposed by the turbine on the cycle are pointed out. In fact, by imposing a treated flow rate, the turbine greatly reduces the flexibility of the cycle. This also has a strong impact on the pressures of the cycle and ultimately on its overall functioning.

5. Conclusions

Given the lack of experimental studies on APC cycles available in literature, the main objective of the present work was the development of a suitable expander for a small scale combined cooling and power production cycle and its integration and testing in an existing single stage ammonia water absorption chiller. The peculiar characteristics of the expander and of the cycle components bring the novelty of the present work.
However, several challenges were faced, mainly related to the small size of the pilot plant. This greatly hindered the choice of expansion device and its development, which was complicated by the corrosiveness of the ammonia-water mixture. Various test campaigns were carried out on the absorption chiller, the turbine (outside and inside the absorption loop) and the combined cycle.

The turbine integrated in the cycle is an impulse axial turbine, in which all expansion takes place in the converging diverging injector. Testing of the single-injector micro-turbine was carried out both inside the experimental loop (using ammonia) and outside the loop, using air, nitrogen and argon.

- Due to the ratio between the injector exit and throat section, the turbine was in choking conditions in all the points tested. Therefore, the linear dependency reported between the turbine inlet pressure and treated mass flow rate is in accordance with theory.

- The consideration of the real-gas behaviour is relevant for the turbine mass flow rate calculation for ammonia (experimental measurements around 10% higher on average than ideal gas computation), while it is negligible for the other tested gases, i.e., nitrogen, argon and air.
- The overall electrical efficiency and power production are strongly correlated to the pressure drop through the turbine and its rotational speed for all fluids tested.
- Because of the small scale of the turbine, and significant losses of the electricity generation components, the maximum electrical efficiency achieved was of 7% and the corresponding optimal rotational speed, 20'000 rpm significantly lower than the expected theoretical value of 50-75'000 rpm.
- Limited influence of the turbine inlet temperature on the overall electrical efficiency was found for the conditions tested.

The integration of the micro-turbine into the single-stage absorption chiller was analysed through an experimental campaign. Tests were conducted only around the nominal operating point of the absorption chiller. Dynamic switching between the three possible operating modes (i.e., cooling, combined cooling and power and only power production in a Kalina cycle configuration) was tested. The measurements bring interesting observations on the functioning of the cycle:

- The lack of possibility to regulate the mass flow rate treated by the turbine imposes strict limits on the cooling production of the bench as it is not possible to change the split ratio between cooling and electrical power production, unless the pressure upstream of the turbine is changed.
- Opening of the turbine line in the nominal point leads to a reduction of the mass flow rate passing through the cooling line of 65% (i.e., split ratio of 0.35) and a cooling power output decrease of around 57% (from 4.9 to 2.1 kW).
- The reduced mass flow rate passing through the cooling line heat exchangers (condenser and evaporator) increases their efficiency, affecting the pressure equilibrium established within the cycle and the circulating vapour mass flow rate (increasing from 16.1 kg/h in the simple absorption working mode to 31.1 kg/h in the combined mode in the nominal operating point).
- Operating mode switching proved to be stable and quick to reach steady state, provided that the starting point was already stable.

Limitations in terms of the operating ranges of the pilot plant and specifically of the turbine (inappropriate design point definition, low efficiency of the electrical generation) did not allow a complete characterisation of the cycle. However, insights and experience gained from the tests will be of paramount importance to continue the development of the technology.
To go further, a numerical model of the cycle based on the gathered experimental data will be developed to evaluate the relevance of the technology on a larger range of operating conditions and scales.

Declaration of Competing Interest

The authors declare that they have no known competing financial interests or personal relationships that could have appeared to influence the work reported in this paper.

Acknowledgements

The authors would like to express their gratitude to the French Alternative Energies and Atomic Energy Commission and the Carnot Energies of the Future Institute. S. Braccio was supported by the CEA NUMERICS program, which has received funding from the European Union Horizon 2020 research and innovation program under the Marie Sklodowska-Curie grant agreement No 800945.
The authors would also like to express their gratitude to Bertrand Chandez, Fabien Bruyat and Florent Lefrançois for their support in the setting up and testing of the machine.

6. References

[1] F. Birol, "The Future of Cooling-Opportunities for energy efficient air conditioning- Opportunities for energy efficient air conditioning," *OECD/IEA 2018*, 2018.

[2] K. E. Herold, R. Radermacher, and S. A. Klein, *Absorption Chillers and Heat Pumps*, Second. CRC Press, 2016.
[3] S. A. Mousavi and M. Mehrpooya, "A comprehensive exergy-based evaluation on cascade absorption-compression refrigeration system for low temperature applications - exergy, exergoeconomic, and exergoenvironmental assessments," *J. Clean. Prod.*, vol. 246, p. 119005, 2020, doi: https://doi.org/10.1016/j.jclepro.2019.119005.
[4] N. Voeltzel, H. T. Phan, Q. Blondel, B. Gonzalez, N. Tauveron, and N. T. N. Voeltzel, H.T. Phan, Q. Blondel, B. Gonzalez, "Steady and dynamical analysis of a combined cooling and power cycle," *Therm. Sci. Eng. Prog.*, vol. 19, no. January, p. 100650, 2020, doi: 10.1016/j.tsep.2020.100650.
[5] E. Fanelli, S. Braccio, G. Pinto, G. Cornacchia, and G. Braccio, "Small scale Organic Rankine Cycle testing for low grade heat recovery by using refrigerants as working fluids," *Model. Meas. Control C*, vol. 79, no. 3, pp. 70–78, 2018, doi: 10.18280/mmc-c.790302.
[6] M. Akbari Kordlar and S. M. S. Mahmoudi, "Exergeoconomic analysis and optimization of a novel cogeneration system producing power and refrigeration," *Energy Convers. Manag.*, vol. 134, pp. 208–220, 2017, doi: 10.1016/j.enconman.2016.12.007.
[7] N. Shokati, F. Ranjbar, and M. Yari, "A comprehensive exergoeconomic analysis of absorption power and cooling cogeneration cycles based on Kalina, part 1: Simulation," *Energy Convers. Manag.*, vol. 158, no. November 2017, pp. 437–459, 2018, doi: 10.1016/j.enconman.2017.12.086.
[8] H. Ghaebi, T. Parikhani, and H. Rostamzadeh, "Energy, exergy and thermoeconomic analysis of a novel combined cooling and power system using low-temperature heat source and LNG cold energy recovery," *Energy Convers. Manag.*, vol. 150, pp. 678–692, 2017, doi: https://doi.org/10.1016/j.enconman.2017.08.052.
[9] W. Huang, J. Wang, J. Xia, P. Zhao, and Y. Dai, "Performance analysis and optimization of a combined cooling and power system using low boiling point working fluid driven by engine waste heat," *Energy Convers. Manag.*, vol. 180, pp. 962–976, 2019, doi: https://doi.org/10.1016/j.enconman.2018.11.041.
[10] D. S. Ayou, J. C. Bruno, R. Saravanan, and A. Coronas, "An overview of combined absorption power and cooling cycles," *Renewable and Sustainable Energy Reviews*, vol. 21. Elsevier, pp. 728–748, 2013, doi: 10.1016/j.rser.2012.12.068.
[11] G. Tamm and D. Y. Goswami, "Novel combined power and cooling thermodynamic cycle for low temperature heat sources, part II: Experimental investigation," *J. Sol. Energy Eng. Trans. ASME*, vol. 125, no. 2, pp. 223–229, 2003, doi: 10.1115/1.1564080.
[12] W. Han *et al.*, "Experimental studies on a combined refrigeration/power generation system activated by low-grade heat," *Energy*, vol. 74, pp. 59–66, 2014, doi: https://doi.org/10.1016/j.energy.2014.02.097.
[13] G. P. Kumar, R. Saravanan, and A. Coronas, "Experimental studies on combined cooling and power system driven by low-grade heat sources," *Energy*, vol. 128, pp. 801–812, 2017, doi: 10.1016/j.energy.2017.04.066.
[14] N. Voeltzel, H. T. Phan, Q. Blondel, B. Gonzalez, and N. Tauveron, "Steady and dynamical analysis of a combined cooling and power cycle," *Therm. Sci. Eng. Prog.*, vol. 19, no. July, p. 100650, 2020, doi: 10.1016/j.tsep.2020.100650.
[15] Q. Blondel, N. Tauveron, N. Caney, and N. Voeltzel, "Experimental study and optimization of the Organic Rankine Cycle with pure NovecTM649 and zeotropic mixture NovecTM649/HFE7000 as working fluid," *Appl. Sci.*, 2019, doi: 10.3390/app9091865.
[16] A. Landelle, N. Tauveron, R. Revellin, P. Haberschill, S. Colasson, and V. Roussel, "Performance investigation of reciprocating pump running with organic fluid for organic Rankine cycle," *Appl. Therm. Eng.*, vol. 113, pp. 962–969, 2017, doi: 10.1016/j.applthermaleng.2016.11.096.
[17] F. Boudéhenn, H. Demasles, J. Wyttenbach, X. Jobard, D. Chèze, and P. Papillon, "Development of a 5 kW cooling capacity ammonia-water absorption chiller for solar cooling applications," *Energy Procedia*, vol. 30, pp. 35–43, 2012, doi: 10.1016/j.egypro.2012.11.006.
[18] D. Triché, S. Bonnot, M. Perier-Muzet, F. Boudéhenn, H. Demasles, and N. Caney, "Experimental and numerical study of a falling film absorber in an ammonia-water absorption chiller," *Int. J. Heat Mass Transf.*, vol. 111, pp. 374–385, 2017, doi: 10.1016/j.ijheatmasstransfer.2017.04.008.
[19] M. Wirtz, "Development of a falling-film desorber combining vapor generation and purification for ammonia–water absorption chiller (Modeling and Experiments), PhD Thesis, Université Savoie Mont Blanc," 2022.
[20] M. Wirtz, B. Stutz, H. T. Phan, and F. Boudehenn, "Combined generator for an NH3–H2O absorption chiller," *Int. J. Heat Mass Transf.*, vol. 196, p. 123311, 2022, doi: https://doi.org/10.1016/j.ijheatmasstransfer.2022.123311.
[21] S. Braccio *et al.*, "Simulation of an ammonia-water absorption cycle using exchanger effectivness.," *Appl. Therm. Eng.*, vol. 213, p. 1, 2022, doi: https://doi.org/10.1016/j.applthermaleng.2022.118712.
[22] N. Tauveron, S. Colasson, and J. A. Gruss, "Available systems for the conversion of waste heat to

electricity," in *ASME International Mechanical Engineering Congress and Exposition, Proceedings (IMECE)*, 2014, doi: 10.1115/IMECE2014-37984.

[23] V. Lemort, S. Quoilin, C. Cuevas, and J. Lebrun, "Testing and modeling a scroll expander integrated into an Organic Rankine Cycle," *Appl. Therm. Eng.*, vol. 29, no. 14–15, pp. 3094–3102, 2009, doi: 10.1016/j.applthermaleng.2009.04.013.

[24] L. C. Mendoza, J. Navarro-Esbrí, J. C. Bruno, V. Lemort, and A. Coronas, "Characterization and modeling of a scroll expander with air and ammonia as working fluid," *Appl. Therm. Eng.*, vol. 70, no. 1, pp. 630–640, 2014, doi: 10.1016/j.applthermaleng.2014.05.069.

[25] O. E. Balje, "A Study on Design Criteria and Matching of Turbomachines: Part A - Similarity relations and Design Criteria of Turbines," *J. Eng. Gas Turbines Power*, vol. 84, no. 1, pp. 83–102, 1962, doi: https://doi.org/10.1115/1.3673386.

[26] S. Braccio, A. Di Nardo, G. Calchetti, H. T. Phan, N. Le Pierrès, and N. Tauveron, "Performance evaluation of a micro partial admission impulse axial turbine in a combined ammonia-water cooling and electricity absorption cycle," *Energy*, p. 127838, 2023, doi: https://doi.org/10.1016/j.energy.2023.127838.

[27] H. G. Lee, J. H. Shin, C. H. Choi, E. Jeong, and S. Kwon, "Partial admission effect on the performance and vibration of a supersonic impulse turbine," *Acta Astronaut.*, vol. 145, no. January, pp. 105–115, 2018, doi: 10.1016/j.actaastro.2018.01.025.

[28] S. Dixon and C. Hall, *Fluid Mechanics and Thermodynamics of Turbomachinery*, Seventh Ed. Butterworth-Heinemann, 2014.

[29] A. Landelle, N. Tauveron, P. Haberschill, R. Revellin, and S. Colasson, "Organic Rankine cycle design and performance comparison based on experimental database," *Appl. Energy*, 2017, doi: 10.1016/j.apenergy.2017.04.012.

[30] H. Saravanamuttoo, G. Rogers, H. Cohen, and P. Straznicky, *Gas Turbine Theory*, 6th ed. Harlow, England; New York: Pearson Prentice Hall, 2009.

[31] S. Braccio, H. T. Phan, N. Tauveron, N. Le Pierrès, and A. Arteconi, "Energy, exergy and exergoeconomic analysis and optimisation of the scale-up of a combined ammonia-water absorption pilot plant producing electricity and refrigeration," *Energy Convers. Manag.*, vol. 278, p. 116686, 2023, doi: https://doi.org/10.1016/j.enconman.2023.116686.